J. Fluid Mech. (1988), *vol.* 188, *pp.* 585–598
Printed in Great Britain

On wavy instabilities of the Taylor-vortex flow between corotating cylinders

By MASATO NAGATA

Department of Mathematical Sciences, University of St. Andrews, North Haugh, St Andrews KY16 9SS, Fife, Scotland

(Received 10 December 1986 and in revised form 1 August 1987)

At least four wavy instabilities are found numerically by analysing the linear stability of Taylor-vortex flow (TVF) in the limit of a small gap between two concentric cylinders which rotate differentially in the same direction. Two of the wavy instabilities, including the one leading to conventional wavy vortex (WVF), have the same axial wavelength as TVF at the onset of instability, while the other two are characterized by subharmonic modes with axial wavelengths twice as long as those of TVF. The two subharmonic instabilities appear to correspond to the wavy-inflow-boundary flow (WIB) and the wavy-outflow-boundary flow (WOB) observed in the experiment of Andereck, Liu & Swinney (1986). The phase velocities, measured in the rotating frame of reference, of all the wavy instabilities are non-zero at the onset except that the phase velocity of WVF vanishes in the region where the average rotation rate Ω of the cylinders is small. By using this *simple bifurcation* property of WVF for small Ω, time-independent finite-amplitude non-axisymmetric solution branches bifurcating from TVF are followed numerically. The most interesting findings are that some of the solution branches cross the line $\Omega = 0$, producing three-dimensional nonlinear solutions in plane Couette flow.

1. Introduction

It is well known that a circular Couette system is one of the most suitable systems for examining bifurcation mechanisms in fluid motions, both experimentally and theoretically. In recent years, particular attention has been paid to the case where both the inner and outer cylinders rotate independently in the same direction. After the experimental discovery of five new flows in the case with corotating cylinders by Andereck, Dickmann & Swinney (1983), who used an apparatus with an aspect ratio $\Gamma = 30$ and with a radius ratio $q = 0.883$, Nagata (1986) obtained numerically two different types of non-axisymmetric solutions bifurcating from Taylor-vortex flow (TVF) by applying periodic conditions in the axial direction. Since Nagata (1986, to be referred by I hereinafter) treated the problem in the limit of a narrow gap and a small angular velocity difference between the cylinders, the best agreement with the experiments was expected in the region close to the Rayleigh line, which implies the stability boundary for circular Couette flow of inviscid fluid. In fact, one of the types of finite-amplitude solutions found in I appears to be the twisted Taylor-vortex flows (TTF) of the experiment of Andereck *et al.* (1983), although the experimental counterpart of the other type is not known. Let us note that very recently Iooss (1986) showed mathematically how the newly observed flows, such as wavy vortex flow (WVF), TTV, wavy inflow boundary (WIB) and wavy outflow boundary

(WOB), resulted from symmetry-breaking phenomena when they bifurcated from TVF. His amplitude expansion procedure was based on the symmetry structure each flow possesses.

Since all the five new flows observed in the experiment manifested themselves in the vicinity of the Rayleigh line, the investigation in I was concentrated on cases for which $\Omega/\mathscr{R}$ is close to the Rayleigh line given by $\Omega/\mathscr{R} = 1$, where $\mathscr{R}$, the Reynolds number, represents the shear strength between the cylinders and Ω, the Coriolis parameter, measures the average rotation rate of the system (for the definitions of $\mathscr{R}$ and Ω, see I (6) and I (7), where the prefix I refers to the paper I). Here, encouraged by the more comprehensive survey of the circular Couette system with corotating cylinders recently performed by Andereck, Liu & Swinney (1986) for a wider range of parameter space, the linear stability analysis on TVF is attempted in the case where $\Omega/\mathscr{R}$ is not necessarily close to 1 by using the computational codes which were used in I. Obviously, the assumption employed in I in order to justify the use of the rectangular coordinate system is not necessarily well founded in the present investigation, especially when $\Omega/\mathscr{R}$ is very small, for the assumption implies that

$$\frac{\Omega}{\mathscr{R}} \gg \frac{D}{\bar{R}} = \frac{2(1-q)}{1+q}, \tag{1}$$

where D and $\bar{R}$ are the dimensional gap and mean radius of the cylinders.†

Nevertheless, in the region far from the Rayleigh line $\Omega/\mathscr{R} = 1$, the onsets of the four wavy instabilities, to be described in detail in the following sections, agree quite well with the experimental observations. In order to provide some evidence for numerical convergence, results for two successive truncation levels (14) with $m = 0$ are compared in figure 1. The number of finite-amplitude components of TVF and the number of infinitesimal perturbation modes superimposed on TVF are 38 and 128 for $(N_T, N_T') = (8, 6)$, while they are 56 and 198, respectively, for $(N_T, N_T') = (10, 7)$, in general. The number of infinitesimal perturbation modes can be approximately halved when one of the symmetries described in detail in I and briefly in the next section is not lost. In spite of the fact that $\Omega/\mathscr{R}$ is not necessarily close to 1, the agreement with the experimental observations is satisfactory for $(N_T, N_T') = (10, 7)$ as is seen in figure 2.

† In terms of the inner- and outer-cylinder Reynolds numbers $\mathscr{R}_i$ and $\mathscr{R}_o$ defined by Andereck *et al.* (1983), the Rayleigh line is given by

$$\mathscr{R}_i/\mathscr{R}_o = q(3-q)/(3q-1)$$

and the assumption mentioned above is equivalent to

$$(\mathscr{R}_i/\mathscr{R}_o + q)/(\mathscr{R}_i/\mathscr{R}_o - q) \gg 1.$$

The inequality is well satisfied only when $\mathscr{R}_i/\mathscr{R}_o = q + \Delta$ $(0 < \Delta \ll 1)$, which differs only slightly from the Rayleigh line $\mathscr{R}_i/\mathscr{R}_o = 1 + \delta$ when the gap is small, i.e. $\delta \equiv 1 - q \ll 1$.

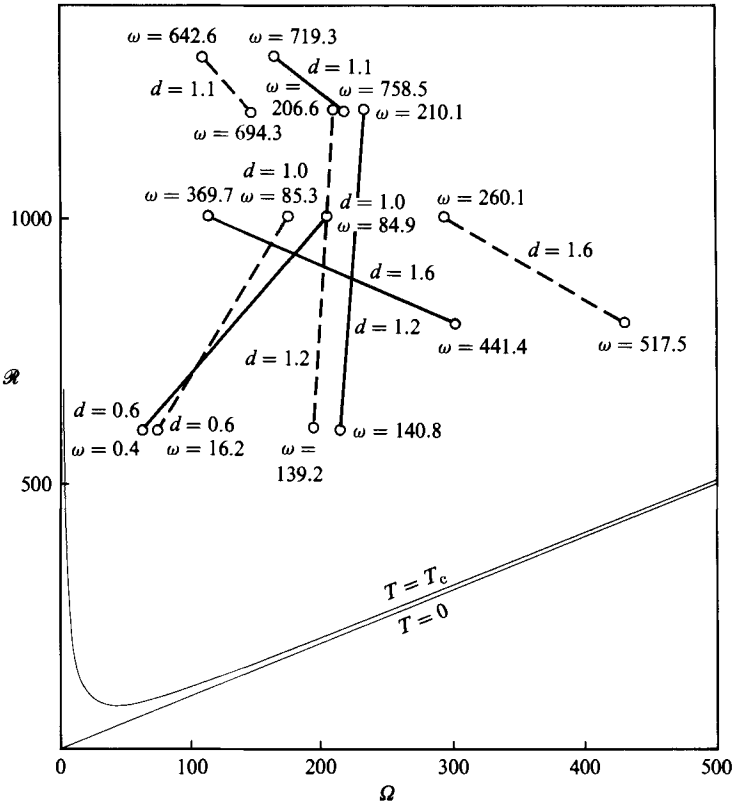

FIGURE 1. The comparison of the onset of the four wavy instabilities between two successive truncation levels $(N_T, N_T') = (8, 6)$ indicated by dashed lines and $(N_T, N_T') = (10, 7)$ indicated by solid lines. In each case two end points, where the values of d and ω are indicated, are simply connected by a straight line. The neutral curve $T = T_c$ is shown as a thin curve whereas the Rayleigh line $T = 0$ is indicated by a thin straight line.

2. The basic symmetry of the problem

The motion of a viscous incompressible fluid between almost corotating cylinders with a narrow gap is governed by

$$\nabla^4 \Delta_2 \phi = \Omega \partial_z \Delta_2 \psi + (-\mathscr{R}x + \check{V}) \partial_y \nabla^2 \Delta_2 \phi - \partial_{xx}^2 (-\mathscr{R}x + \check{V}) \partial_y \Delta_2 \phi + \hat{\boldsymbol{i}} \cdot \nabla \times \nabla \times [\check{\boldsymbol{u}} \cdot \nabla \check{\boldsymbol{u}}] + \partial_t \nabla^2 \Delta_2 \phi, \quad (2a)$$

$$\nabla^2 \Delta_2 \psi = -\Omega \partial_z \Delta_2 \phi + (-\mathscr{R}x + \check{V}) \partial_y \Delta_2 \psi - \partial_x (-\mathscr{R}x + \check{V}) \partial_z \Delta_2 \phi - \hat{\boldsymbol{i}} \cdot \nabla \times [\check{\boldsymbol{u}} \cdot \nabla \check{\boldsymbol{u}}] + \partial_t \Delta_2 \psi, \quad (2b)$$

$$\partial_t \check{V} - \partial_{xx}^2 \check{V} = \partial_x \overline{\Delta_2 \phi (\partial_{xy}^2 \phi + \partial_z \psi)}, \quad (2c)$$

where $\Delta_2 = \partial_{yy}^2 + \partial_{zz}^2$ and the bar denotes a yz-average (see I (13)). The scalars ϕ and ψ are the poloidal and toroidal parts, respectively, of a solenoidal velocity disturbance $\check{\boldsymbol{u}}$, whereas $\check{V}$ denotes the modification of the mean flow from the circular Couette solution $V = -\mathscr{R}x$. Thus, the total velocity $\boldsymbol{u}$ is given by

$$\boldsymbol{u} = (-\mathscr{R}x + \check{V})\hat{\boldsymbol{j}} + \nabla \times (\nabla \times \hat{\boldsymbol{i}} \phi) + \nabla \times \hat{\boldsymbol{i}} \psi, \quad (3)$$

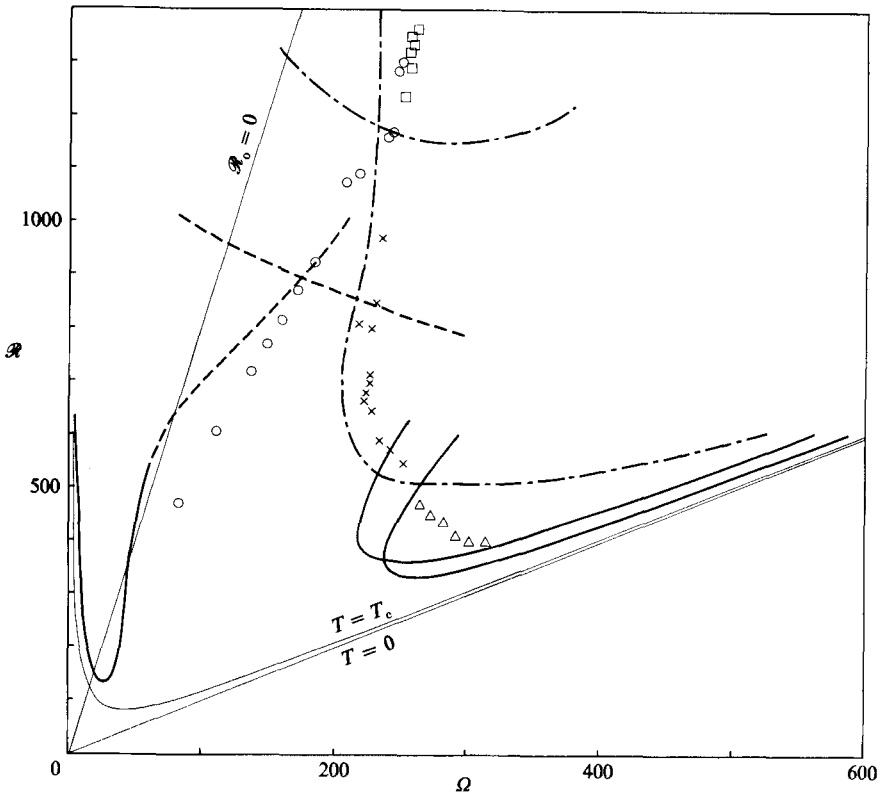

FIGURE 2. The stability diagram of TVF. The onset of time-independent instabilities are shown by solid curves, whereas the onset of time-dependent instabilities are shown by either dashed curves (WVF1 and WVF2) or dash-dotted curves (SUBL and SUBH). ○, WVF; ×, WOB; □, WIB; △, TTV, observed by Andereck *et al.* (1986).

where the unit vectors $\hat{\boldsymbol{\imath}}$ and $\hat{\boldsymbol{\jmath}}$ correspond to the radial direction x and the azimuthal direction y, respectively. The prescribed no-slip boundary conditions at $x = \pm\frac{1}{2}$ are

$$\phi = \partial_x \phi = \psi = \check{V} = 0. \tag{4}$$

Assuming infinite extent in the axial direction z, we first seek an axisymmetric finite-amplitude solution of the form

$$\phi = \sum_{l=1}^{\infty} \sum_{n=-\infty}^{\infty} a_{ln} \mathrm{e}^{\mathrm{i}n\gamma z} f_l(x), \tag{5a}$$

$$\psi = \sum_{l=1}^{\infty} \sum_{n=-\infty}^{\infty} b_{ln} \mathrm{e}^{\mathrm{i}n\gamma z} g_l(x), \tag{5b}$$

$$\check{V} = \sum_{k=1}^{\infty} c_k \sin 2k\pi x, \tag{5c}$$

where f_l and g_l are the sets of orthogonal functions (see I (23)) satisfying (4). The solution, called Taylor-vortex flow (TVF), is steady with respect to a frame of reference rotating with the angular velocity Ω and is known to bifurcate supercritically from the circular Couette flow when the Taylor number

$T = \Omega(\mathscr{R}-\Omega) = 1708$ with an axial wavenumber $\gamma = 3.117$. Only the case with $\gamma = 3.117$ will be considered.

Because of the assumption of a narrow gap between almost corotating cylinders, the system (2) has a special symmetry property of invariance with respect to the point symmetry on the horizontal plane,

$$Qu(x,y,z) = [-u(-x,-y,z), -v(-x,-y,z), w(-x,-y,z)], \tag{6a}$$

in addition to the ordinary symmetry property which the circular Couette system usually has. They are the property of invariance under translations along the axial direction z, reflections through the horizontal plane, and rotations about the z-axis and are expressed in terms of Iooss' (1986) notation as follows:

$$\tau_\zeta u(x,y,z) = u(x,y,z+\zeta), \tag{6b}$$

$$Su(x,y,z) = [u(x,y,-z), v(x,y,-z), -w(x,y,-z)], \tag{6c}$$

$$R_\eta u(x,y,z) = u(x,y+\eta,z). \tag{6d}$$

The TVF $\mathscr{U}_0$ (see I (27)) has the following properties:

$$Q\mathscr{U}_0 = \mathscr{U}_0, \quad \tau_{2\pi/\gamma}\mathscr{U}_0 = \mathscr{U}_0, \quad R_\eta \mathscr{U}_0 = \mathscr{U}_0, \quad S\mathscr{U}_0 = \mathscr{U}_0. \tag{7}$$

3. Linear stability analysis

Having obtained TVF solutions by a Galerkin method for the truncated system of nonlinear algebraic equations for a_{ln}, b_{ln} and c_k, derived from (2), stability analysis is performed by superimposing general three-dimensional perturbations on the TVF solutions. The perturbations $\tilde{\phi}$ and $\tilde{\psi}$ have the same periodicity as that of TVF in the axial direction with additional exponential dependences on y, z and t:

$$\tilde{\phi} = \sum_{l=1}^{\infty}\sum_{n=-\infty}^{\infty} \tilde{a}_{ln}\, e^{in\gamma z} f_l(x) \exp i(dy+bz) + \sigma t, \tag{8a}$$

$$\tilde{\psi} = \sum_{l=1}^{\infty}\sum_{n=-\infty}^{\infty} \tilde{b}_{ln}\, e^{in\gamma z} g_l(x) \exp i(dy+bz) + \sigma t. \tag{8b}$$

After orthogonalizing the equations, the resulting eigenvalue problem with σ as the time growth rate is solved numerically for each pair of Floquet parameters d and b by the matrix inversion method.

The growth rates σ with the biggest real part are listed for the typical parameter values $\mathscr{R} = 600$ and $\Omega = 240$ in table 1. Several things should be noted about the table. First, perturbations are separated into two classes $\tilde{\mathscr{U}}_{\mathrm{I}}$ and $\tilde{\mathscr{U}}_{\mathrm{II}}$ (see I (33a, b)) only when $b = 0$. For $b \neq 0$, perturbations belonging to different classes interact with each other through TVF of the class $\mathscr{U}_0$. Secondly, σ in table 1 as a function of d and b is smooth only locally, because different modes may be associated with the eigenvalue σ with the biggest real part for different values of d and b. Thirdly, discrepancies between the values of σ at $b = \gamma$ and σ with a bigger real part at $b = 0$ are due to the finite truncation level. For an infinite truncation level, σ must be strictly periodic in b with period γ. As a matter of fact, these discrepancies serve as a tool for checking the accuracy with respect to the truncation level. They seem to be small enough at the truncation level $(N_{\mathrm{T}}, N'_{\mathrm{T}}) = (10, 7)$ as shown in table 1 and calculations are performed all through this section using this truncation level. Lastly

$d\backslash b$	...	0	0.779	1.559	2.338	3.117
0	−20.00, ±226.6	0, 0	−1.76, 0	−5.67, 0	−0.90, 0	−2.17, 0
1.0	−37.71, ±157.2	−19.29, ±137.0	−8.15, ±143.5	0.95, ±147.9	−3.79, ±143.8	−19.95, ±139.2
2.0	−37.80, ±116.4	−41.66, ±357.8	−35.75, ±372.9	−29.42, ±383.9	−39.49, ±375.5	−37.63, ±116.2
3.0	−21.65, 0	−67.22, ±69.8	−40.23, ±249.6	−26.92, ±361.6	−37.85, 0	−21.00, 0
4.0	−4.97, 0	−78.89, ±4.4	−10.91, 0	−22.93, ±7.9	−8.44, 0	−3.91, 0
5.0	−19.78, 0	−60.50, 0	−23.79, 0	−34.48, ±0.6	−22.67, 0	−19.07, 0
6.0	−49.12, 0	−97.42, ±11.3	−52.66, 0	−63.00, ±1.2	−52.36, 0	−48.72, 0
Class	$\tilde{U}_{\mathrm{I}}$	$\tilde{U}_{\mathrm{II}}$	$\tilde{U}_{\mathrm{I}}+\tilde{U}_{\mathrm{II}}$			

TABLE 1. The growth rate σ as a function of the Floquet parameters d and b. The second figure in each pair corresponds to the frequency $\omega = \mathrm{Im}[\sigma]$ for the eigenvalue with the biggest real part indicated by the first figure. $\mathscr{R} = 600$, $\Omega = 240$.

perturbations with $d = b = 0$ must have zero growth rate, because the special perturbations given by

$$\tilde{\phi} = \frac{\partial \phi}{\partial z}, \quad \tilde{\psi} = \frac{\partial \psi}{\partial z} \tag{9}$$

correspond to an infinitesimal translation of TVF ϕ, ψ in the z-direction and thus are solutions of the stability equations. From the expression of the class $\mathscr{U}_0$ for TVF and differentiation of ϕ or ψ by z, it is clear that perturbations in class $\tilde{\mathscr{U}}_{\mathrm{II}}$ are responsible for this translation instability.

Two local peaks can be recognized in table 1: one at $b = \frac{1}{2}\gamma$, $d = 1$ which will be discussed in §3.1 and the other at $b = 0$, $d = 4$ from the class $\tilde{\mathscr{U}}_{\mathrm{I}}$. The latter is related to the twisted Taylor-vortex flow reported in I, although the peak is negative for the particular parameter values chosen for table 1. The classes $\tilde{\mathscr{U}}_{\mathrm{I}}$ and $\tilde{\mathscr{U}}_{\mathrm{II}}$ satisfy

$$S\tilde{\mathscr{U}}_{\mathrm{I}} = \tilde{\mathscr{U}}_{\mathrm{I}}, \quad \tau_{2\pi/\gamma}\tilde{\mathscr{U}}_{\mathrm{I}} = \tilde{\mathscr{U}}_{\mathrm{I}}, \tag{10a}$$

$$S\tilde{\mathscr{U}}_{\mathrm{II}} = -\tilde{\mathscr{U}}_{\mathrm{II}}, \quad \tau_{2\pi/\gamma}\tilde{\mathscr{U}}_{\mathrm{II}} = \tilde{\mathscr{U}}_{\mathrm{II}} \tag{10b}$$

respectively (see Iooss 1986, p. 252).

3.1. *Subharmonic instabilities*

Wavy instabilities with a subharmonic mode were first detected numerically by Jones (1985) in the case with the outer cylinder at rest by setting the wavelength of perturbations equal to an integer multiple of that of the axisymmetric TVF. Here, instead of expecting a subharmonic instability *a priori*, the growth rate σ is evaluated by regarding it as a continuous function of d and b. As a result, a subharmonic instability is actually found at $b = \frac{1}{2}\gamma$ as seen in table 1, although table 1 exhibits σ only at selected values of d and b. The peak $\sigma = (4.83 \pm 143.4\mathrm{i})$ on

$b = \frac{1}{2}\gamma$ occurs at $d = 1.23$ when $\mathscr{R} = 600$ and $\Omega = 240$. This subharmonic instability (SUBL) bounds the stability region of TVF from the right in the $(\Omega, \mathscr{R})$-plane, almost without any change in the critical value of Ω ($205 < \Omega < 230$) at the onset of instability when $\mathscr{R} > 530$, as seen in figure 2. For $\mathscr{R} < 530$, the instability in the class $\tilde{\mathscr{U}}_{\mathrm{I}}$ associated with TTV becomes dominant. Along the curve of onset of SUBL, the value of d is almost constant ($d \approx 1.2$), while the frequency $\omega \equiv \mathrm{Im}[\sigma]$ varies from 120 at the bottom of the curve around $\mathscr{R} = 510$ to 210 at $\mathscr{R} = 1200$.

It is found that when $\mathscr{R} \approx 1200$ two additional subharmonic instabilities appear. Only one of them, which occurs at $\Omega = 220$, is shown in both figure 1 and figure 2, since the other subharmonic instability that appears at $\Omega = 270$ intersects the curve of onset of SUBL at a higher value of $\mathscr{R}$. In contrast to the relatively low frequencies, $\omega \approx 200$, associated with SUBL, the new subharmonic instability SUBH has higher frequencies ($\omega \approx 750$). Along the curve of onset of SUBH, the value of d is almost unchanged ($d \approx 1.1$) as well and is close to $d = 1.2$ for SUBL.

The comparison with the experimental observations by Andereck *et al.* (1986) illustrated in figure 2 indicates that the two subharmonic instabilities SUBL and SUBH correspond to WOB and WIB, respectively, although the curve of onset of SUBH is slightly tilted backward towards the line $\Omega = 0$ for higher $\mathscr{R}$. It is found that the values of d for SUBL and SUBH are consistent with the observed waves ($M = 11 \sim 14$) around cylinders by the relation (I (40))

$$\beta = \frac{MD}{\bar{R}} = 0.124M. \tag{11}$$

It might be thought that by expressing $\mathrm{e}^{\mathrm{i}n\gamma z}\,\mathrm{e}^{\mathrm{i}\frac{1}{2}\gamma z}$ in trigonometric functions, subharmonic perturbation modes could be represented by the following two classes:

$$\tilde{\mathscr{U}}^{(\mathrm{i})} = \left[\tilde{\phi}: \cos n^{+}\tfrac{1}{2}\gamma z \begin{Bmatrix} f_{\mathrm{a}}(x) \\ f_{\mathrm{s}}(x) \end{Bmatrix}, \quad \tilde{\psi}: \sin n^{+}\tfrac{1}{2}\gamma z \begin{Bmatrix} f_{\mathrm{a}}(x) \\ f_{\mathrm{s}}(x) \end{Bmatrix}\right]$$

and

$$\tilde{\mathscr{U}}^{(\mathrm{ii})} = \left[\tilde{\phi}: \sin n^{+}\tfrac{1}{2}\gamma z \begin{Bmatrix} f_{\mathrm{a}}(x) \\ f_{\mathrm{s}}(x) \end{Bmatrix}, \quad \tilde{\psi}: \cos n^{+}\tfrac{1}{2}\gamma z \begin{Bmatrix} f_{\mathrm{a}}(x) \\ f_{\mathrm{s}}(x) \end{Bmatrix}\right],$$

where n^{+} denotes an odd integer, and f_{a} and f_{s} represent antisymmetric and symmetric functions in x, respectively. Knowing that the class $\mathscr{U}_0$ for TVF could be written as

$$\mathscr{U}_0 = \left[\phi: \begin{Bmatrix} \cos 2n^{++}\tfrac{1}{2}\gamma z f_{\mathrm{a}}(x) \\ \cos 2n^{+}\tfrac{1}{2}\gamma z f_{\mathrm{s}}(x) \end{Bmatrix}, \quad \psi: \begin{Bmatrix} \sin 2n^{++}\tfrac{1}{2}\gamma z f_{\mathrm{a}}(x) \\ \sin 2n^{+}\tfrac{1}{2}\gamma z f_{\mathrm{s}}(x) \end{Bmatrix}\right],$$

where n^{++} stands for an even integer, one would imagine, with a necessary translation in z, that the two classes could be distinguished by the property that the wavy boundaries between vortices would coincide with either the inflow or the outflow boundaries of TVF, since the axial component of the velocity, w, is given by $\partial^2_{zx}\phi - \partial_y\psi$ so that one boundary would be flat and the other would always be wavy. Actually, the subharmonic classes $\tilde{\mathscr{U}}^{(\mathrm{i})}$ and $\tilde{\mathscr{U}}^{(\mathrm{ii})}$ satisfy relations

$$S\tilde{\mathscr{U}}^{(\mathrm{i})} = \tilde{\mathscr{U}}^{(\mathrm{i})}, \quad \tau_{2\pi/\gamma}\tilde{\mathscr{U}}^{(\mathrm{i})} = -\tilde{\mathscr{U}}^{(\mathrm{i})}, \tag{12a}$$

$$S\tilde{\mathscr{U}}^{(\mathrm{ii})} = -\tilde{\mathscr{U}}^{(\mathrm{ii})}, \quad \tau_{2\pi/\gamma}\tilde{\mathscr{U}}^{(\mathrm{ii})} = -\tilde{\mathscr{U}}^{(\mathrm{ii})}, \tag{12b}$$

which are used in the definitions for WIB and WOB by Iooss (1986). However, the perturbation modes are separable only for $b = 0$, and not, as one might think, for $b = \frac{1}{2}\gamma$. The two classes, $\tilde{\mathscr{U}}^{(\mathrm{i})}$ and $\tilde{\mathscr{U}}^{(\mathrm{ii})}$, represent the same solution because of the

symmetry property (6a) which the present problem possesses in the particular limit considered. The subharmonic instabilities are associated with a pitchfork bifurcation. Curvature is required in order to break the symmetry and locally transform the bifurcation picture into one with a transcritical bifurcation at the bifurcation point. Nonlinear analysis cannot resolve the inseparability of the subharmonic instabilities. The situation is similar to the problem of Boussinesq convection, where the inclusion of the second volume expansion coefficient only enables the separation of the 1-hexagon and g-hexagon solutions (Busse 1978).

3.2. *Wavy vortex flows*

Two instabilities with $\mathrm{Im}\,[\sigma] \neq 0$, classified as WVF1 and WVF2 in figure 2 are found on $b = 0$. In contrast to TTV, described in I, perturbations in the class $\tilde{\mathscr{U}}_{\mathrm{II}}$ are responsible for the instabilities. Hence both WVF1 and WVF2 have not only wavy inflow but also wavy outflow boundaries and they propagate their wavy patterns in the azimuthal direction without changing their axial wavelengths when they bifurcate from TVF.

WVF2 is characterized by rather high frequencies ($\omega \approx 400$) and bounds the stability region of TVF from above in the $(\Omega, \mathscr{R})$-plane (see figure 2). The other wavy instability WVF1, described by relatively low frequencies, bounds the stable TVF from the region where Ω is small. Although WVF1 and WVF2 are clearly distinguished by the value of d at the onset of instability in addition to their distinct frequency differences, it is not possible to pinpoint a local maximum of the growth rate σ as a function of d for $\mathscr{R} \gtrsim 1100$ because of the presence of several unstable modes in the class $\tilde{\mathscr{U}}_{\mathrm{II}}$. The exact values of d at which the peak of σ occurs are required in order to interpolate the stability boundaries for TVF on which $\mathrm{Re}\,[\sigma]$ changes signs.

A typical graph of $\mathrm{Re}\,[\sigma]$ as a function of Ω is depicted in figure 3 for the low-frequency wavy instability WVF1. It is seen that the Hopf bifurcation point at $\Omega = \Omega_{\mathrm{H}}$ and the simple bifurcation point at $\Omega = \Omega_2$ on the lower real eigenvalue branch are very close in the figure. As $\mathscr{R}$ is decreased from 600, the whole graph is shifted downward, making the distance between Ω_{H} and Ω_2 much smaller. Consequently, the frequency $\omega = \mathrm{Im}\,[\sigma]$ at $\Omega = \Omega_{\mathrm{H}}$ approaches zero until the simple bifurcation moves on to the upper real eigenvalue branch at $\mathscr{R} \sim 550$, leaving the branching point, where the complex-conjugate eigenvalues change into two real eigenvalues, beneath the line of zero growth rate. Therefore, the transition from TVF is time-independent or time-dependent according to whether $\mathscr{R} < 550$ or $\mathscr{R} > 550$. At $\Omega = \Omega_{\mathrm{o}}$, where TVF bifurcates supercritically from a circular Couette flow, the eigenvalues on the upper and the lower real eigenvalue branches are both negative. Hence, there is a small interval between $\Omega = \Omega_{\mathrm{o}}$ and another simple bifurcation point at $\Omega = \Omega_1$, where TVF is stable with respect to infinitesimal perturbations.

The comparison with the experiments of Andereck *et al.* (1986) shows that WVF1 corresponds to the conventional WVF (see figure 2). They also give the linear relation between the angular velocity of the wavy patterns and the rotation ratio $\Omega_{\mathrm{o}}/\Omega_{\mathrm{i}} \equiv q\mathscr{R}_{\mathrm{o}}/\mathscr{R}_{\mathrm{i}}$ of the cylinders. By using the transformation formulas I 39a, b), the line $\mathscr{R}_{\mathrm{o}}/\mathscr{R}_{\mathrm{i}} = 1/K$ (K: constant) is mapped into the line

$$\mathscr{R} = \frac{1}{2}\frac{K-q}{K+q}\frac{1+q}{1-q}\Omega \tag{13}$$

in the $(\Omega, \mathscr{R})$-plane. Since the curve of onset of WVF1 makes some angle with lines of $\mathscr{R}/\Omega = \text{constant}$ when $\mathrm{Im}\,[\sigma] \neq 0$, the point on the curve with larger $\mathscr{R}$ corresponds

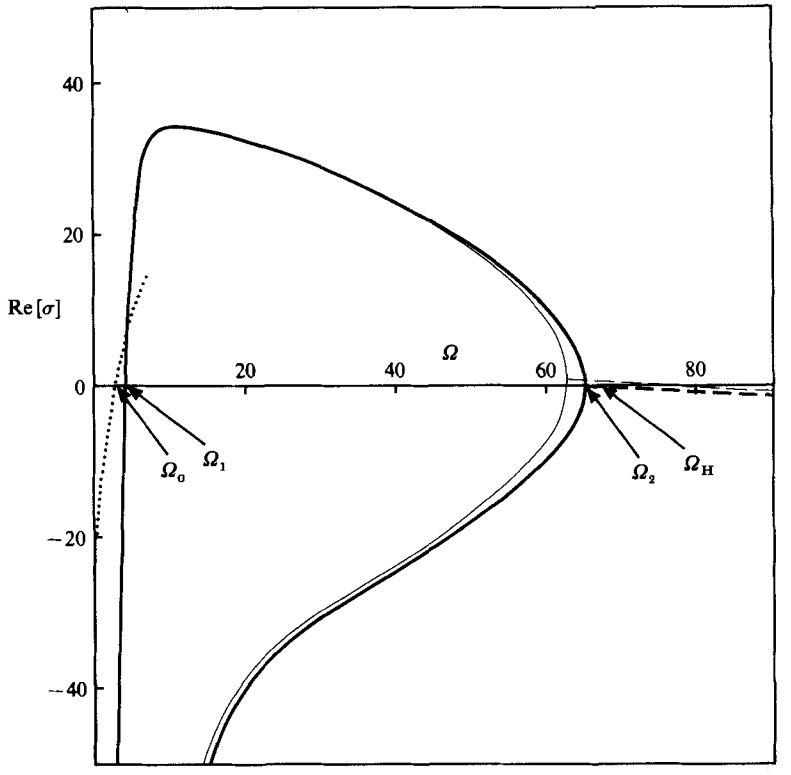

FIGURE 3. The growth rate Re $[\sigma]$ as a function of Ω. Solid curves and dashed curves indicate that the eigenvalue σ is real or complex conjugate, respectively. Thick and thin curves correspond to $(N_T, N_T') = (10, 7)$ and $(8, 6)$, respectively. $\mathscr{R} = 600$, $d = 0.6$. The two-dimensional perturbation ($d = 0$) superimposed on the unidirectional circular Couette flow has the maximum growth rate for $0 < \Omega < \Omega_0$, indicated by a dotted line.

to smaller K. The tendency that Im $[\sigma]$ becomes smaller as $\mathscr{R}$ decreases is consistent with their observations. Also, the value of d at the onset of WVF1 ($0.6 < d < 1.0$) is compatible with the observed number of waves ($M \sim 6$) for WVF (see (11)).

An experimental counterpart of the high-frequency wavy instability WVF2 has not been reported.

4. Nonlinear analysis

The fact that the TVF has two simple bifurcation points at $\Omega = \Omega_1$ and $\Omega = \Omega_2$ provides encouragement for seeking time-independent finite-amplitude non-axisymmetric solutions bifurcating from TVF at each bifurcation point. In particular, when $\mathscr{R} < 550$, a search by numerical methods is expected not to be influenced by time-dependent disturbances because of the suspended Hopf bifurcation. Since the growing perturbations took the form of those in the class $\tilde{\mathscr{U}}_{II}$ in the linear stability analysis, finite-amplitude solutions represented by the class $\mathscr{A}_2$ are responsible for the bifurcation (see Appendix in I).

In order to obtain a solution, initial guesses at the numerical solutions are made near the bifurcation points so that the guesses are slightly different from TVF solutions. The truncation formula I (36), i.e.

$$l + 2|m| + |n| \leqslant N_T, \quad k \leqslant N_T' \tag{14}$$

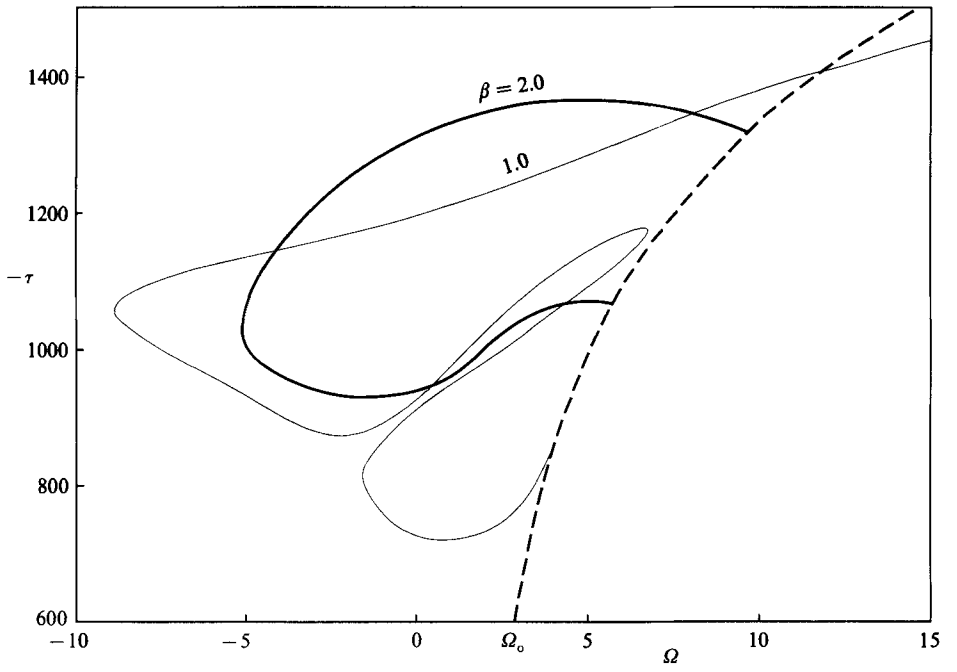

FIGURE 4. The bifurcation picture based on the torque τ. The non-axisymmetric solution branches for $\beta = 1.0$ and $\beta = 2.0$ are shown. The axisymmetric TVF, which exists for $\Omega > \Omega_0 = 2.86$, is indicated by a dashed curve. $\mathscr{R} = 600$.

is used because of the existence of the axisymmetric ($m = 0$) TVF which has been already established ($l + |n| \leqslant N_T$) as a background at the bifurcation of non-axisymmetric flows.

$$\phi = \sum_{l=1}^{\infty} \sum_{m=-\infty}^{\infty} \sum_{n=-\infty}^{\infty} a_{lmn} \exp \mathrm{i}(m\beta y + n\gamma z) f_l(x),$$

$$\psi = \sum_{l=1}^{\infty} \sum_{m=-\infty}^{\infty} \sum_{n=-\infty}^{\infty} b_{lmn} \exp \mathrm{i}(m\beta y + n\gamma z) g_l(x),$$

$$\check{V} = \sum_{k=1}^{\infty} c_k \sin 2k\pi x.$$

The azimuthal wavenumber β is set equal to the value of d for the growing perturbations, while the axial wavenumber γ remains unchanged from its value for TVF solutions because $b = 0$.

It is found that non-axisymmetric solutions bifurcate supercritically at $\Omega = \Omega_2$, while the bifurcation is subcritical at $\Omega = \Omega_1$. Although TVF is found to be most unstable with respect to perturbations with $d = 0.2$ at $\Omega = \Omega_1$ for $\mathscr{R} = 600$, subcritical solutions with shorter wavelengths can be followed further in the direction of negative Ω. Solutions with $0.9 \leqslant \beta \leqslant 2.1$ actually reach the line of plane-Couette-flow limit $\Omega = 0$ directly when $\mathscr{R} = 600$. Figure 4 shows a bifurcation picture based on the torque τ,

$$\tau = \frac{\mathrm{d}}{\mathrm{d}x}(-\mathscr{R}x + \check{V})|_{x=\pm\frac{1}{2}}, \tag{15}$$

exerted on the wall of the cylinders for azimuthal wavenumbers $\beta = 1.0$ and $\beta = 2.0$. As solutions approach a turning point, some non-axisymmetric components with $m \neq 0$ become gradually dominant and beyond the turning point the solutions have

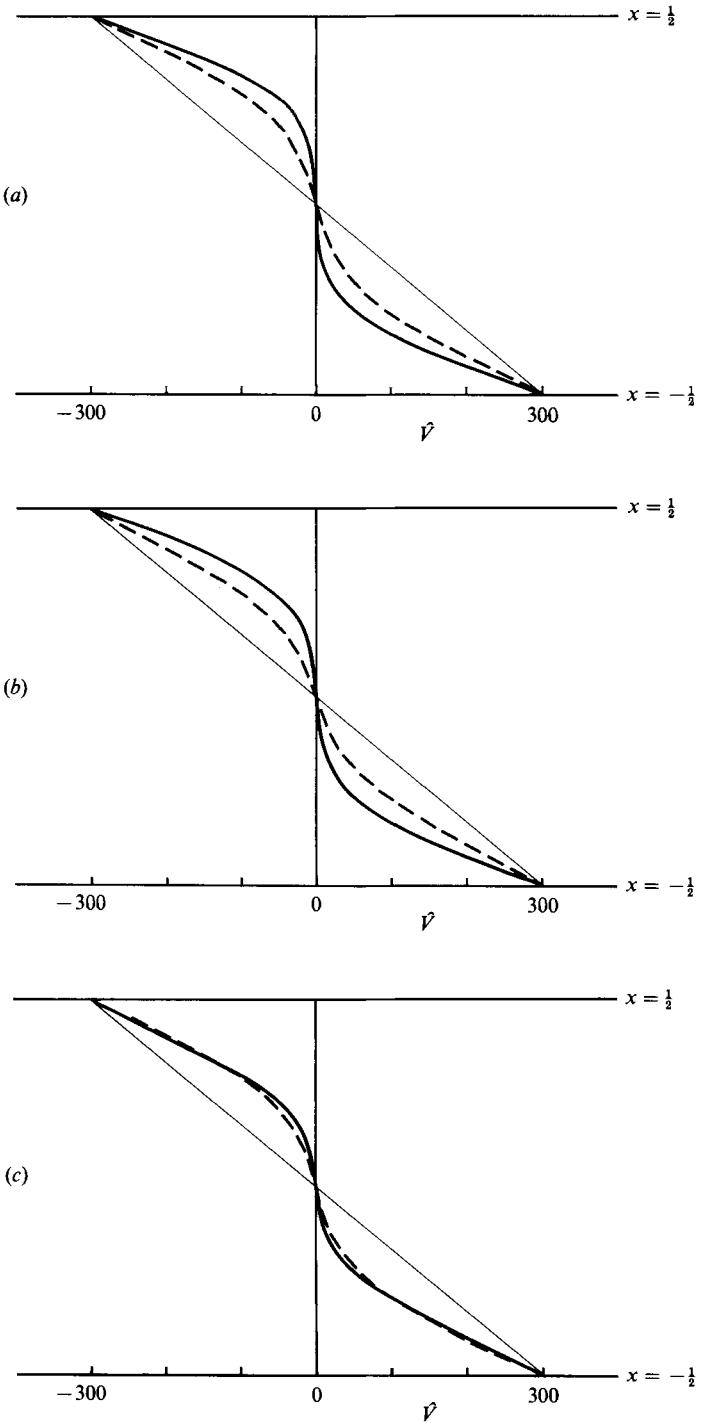

FIGURE 5. The modification of the mean flow $\hat{V}(x) = -\mathscr{R}x + \check{V}(x)$. Solid curves and dashed curves indicate the upper and the lower part, respectively, of the three-dimensional solution branch for $\beta = 2.0$ in figure 4. $\mathscr{R} = 600$. (*a*) $\Omega = 5$, (*b*) 0, (*c*) -5.

different structures as can be seen by the modification of the mean flow in figure 5. Components with higher harmonic indices $l+|m|+|n|$ normally show decreasing orders of magnitude.

Because of the existence of turning points, multiple solutions belonging to the same class $\mathscr{A}_2$ are possible for fixed Ω. For instance, plane Couette flow on $\Omega = 0$ has two and four solutions for $\beta = 2.0$ and $\beta = 1.0$, respectively, when $\mathscr{R} = 600$. The nonlinear aspects of plane-Couette-flow solutions will be reported in a separate paper (Nagata 1988).

5. Conclusion

Comparison between the present numerical investigation and the experimental observations by Andereck *et al.* (1986) is made in figure 2. The onsets of the second bifurcations are in good agreement, except for the high-frequency wavy vortex flow WVF2, where no experimental counterpart is known. The crossing point of the curves of onset for the two subharmonic instabilities SUBL and SUBH, where two Hopf bifurcations meet, is preceded by this WVF2 instability. The bifurcation of WVF2 might be subcritical, and this may be the reason why high-frequency wavy vortex flows have not been detected.

It has already been pointed out that the use of a rectangular coordinate system to solve the narrow-gap problem ($q \ll 1$) cannot be justified when $\Omega/\mathscr{R}$ becomes as small as $D/\bar{R} = 2(1-q)/(1+q) \approx 1-q$. Therefore, our analysis can only qualitatively describe the various events that occur in the case with the outer cylinder at rest and the case of counter-rotating cylinders. The second quadrant in the $\mathscr{R}_o-\mathscr{R}_i$ plane is mapped into the narrow region between the lines

$$\mathscr{R} = \pm\frac{1}{2}\frac{1+q}{1-q}\Omega$$

in the $(\Omega, \mathscr{R})$-plane. Nevertheless, the nonlinear analysis attempted in that narrow area shows mathematically that some solutions bifurcating at $\Omega = \Omega_1$ cross the line $\Omega = \Omega_0$, making possible direct three-dimensional bifurcation from the unidirectional circular Couette flow. Furthermore, some three-dimensional solutions can be traced back into the region of negative Ω. In this region, which corresponds to the region below the line $\mathscr{R}_i = -q\mathscr{R}_o$ in the $(\mathscr{R}_o, \mathscr{R}_i)$-plane, only three-dimensional flows such as spirals, wavy spirals and some turbulent structures have been reported in the experiments.

It should be noted that the mathematical formulation of plane Couette flow can be retrieved simply by considering the limit of $\Omega = 0$ in our analysis without any approximations. All the linear stability analyses for plane Couette flow have indicated that the unidirectional flow $\boldsymbol{u} = \mathscr{R}x\hat{\boldsymbol{i}}$ is stable with respect to infinitesimal perturbations with any normal mode at any Reynolds number. Thus, if transitions from the laminar flow exist they must be abrupt and the secondary solutions resulting from the transition cannot be connected to the undisturbed solutions for all $\mathscr{R}$. The three-dimensional finite-amplitude solutions discovered in the present paper for $\Omega = 0$ could be regarded as solutions bifurcating from the infinite value of $\mathscr{R}$. A simple conjectured bifurcation picture near and on $\Omega = 0$ is provided in figure 6. The idea of a bifurcation from infinity was first proposed by Rosenblat & Davis (1979) and was suggested by Cowley & Smith (1985) for the mixed problem of plane Poiseuille flow and plane Couette flow. But Cowley & Smith's solutions were two-dimensional and existed only when the plane-Poiseuille-flow component was

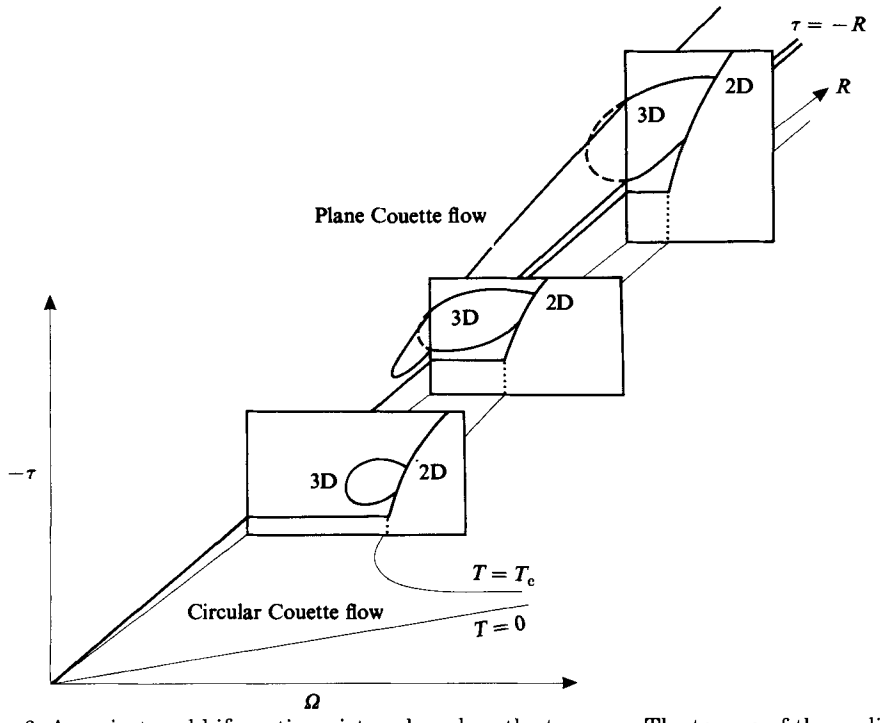

FIGURE 6. A conjectured bifurcation picture based on the torque τ. The torque of the undisturbed flows is given by $\tau = -\mathscr{R}$. The three-dimensional-solution surface will have more complex structures with folds as can be anticipated from its cross-section at $\mathscr{R} = 600$ for $\beta = 1.0$ in figure 4.

dominant. We should also note that Orszag & Kells (1980) demonstrated by their numerical experiments on plane Couette flow that artificially created two-dimensional disturbances decayed eventually whereas three-dimensional disturbances sustained their amplitudes.

The solutions on $\Omega = 0$ have already developed three-dimensional structures. Therefore, the truncation formula

$$l + |m| + |n| \leqslant N_{\mathrm{T}}$$

instead of (14) is more appropriate. Numerical work in that direction is in progress (Nagata 1988). As an extreme truncation, the approach using the triad interaction proposed by Craik (1971) may resolve some basic properties of the stability of plane Couette flow.

For numerical efficiency, only time-independent nonlinear solutions bifurcating from TVF were sought. The Galerkin scheme incorporating the phase velocity must take into account twice as many components compared with the time-independent case considered here. (Because of the non-zero time derivatives, one of the symmetry properties is broken.) It is very likely that inflexional flows as seen in figure 5 become unstable eventually for higher Reynolds numbers. To examine plausible successive time-dependent bifurcations from the steady three-dimensional solution manifolds is very interesting, especially for plane Couette flow, although the numerical cost of solving an initial-value problem is also expected to be expensive.

The author is grateful to Professor F. H. Busse for numerous discussions. This research was supported by SERC.

REFERENCES

ANDERECK, C. D., DICKMAN, R. & SWINNEY, H. L. 1983 New flows in a circular Couette system with co-rotating cylinders. *Phys. Fluids* **26**, 1395–1401.

ANDERECK, C. D., LIU, S. S. & SWINNEY, H. L. 1986 Flow regimes in a circular Couette system with independently rotating cylinders. *J. Fluid Mech.* **164**, 155–183.

BUSSE, F. H. 1978 Non-linear properties of thermal convection. *Rep. Prog. Phys.* **41**, 1927–1967.

COWLEY, S. J. & SMITH, F. T. 1985 On the stability of Poiseuille–Couette flow: a bifurcation from infinity. *J. Fluid Mech.* **156**, 83–100.

CRAIK, A. D. D. 1971 Non-linear resonant instability in boundary layers. *J. Fluid Mech.* **50**, 393–413.

Iooss, G. 1986 Secondary bifurcations of the Taylor vortices into wavy inflow and outflow boundaries. *J. Fluid Mech.* **173**, 273–288.

JONES, C. A. 1985 The transition to wavy Taylor vortices. *J. Fluid Mech.* **157**, 135–162.

NAGATA, M. 1986 Bifurcations in Couette flow between almost corotating cylinders. *J. Fluid Mech.* **169**, 229–250.

NAGATA, M. 1987 Three-dimensional finite amplitude solutions in plane Couette flow. *Phys. Rev.* (submitted).

ORSZAG, S. A. & KELLS, L. C. 1980 Transition to turbulence in plane Poiseuille and plane Couette flow. *J. Fluid Mech.* **96**, 159–206.

ROSENBLAT, S. & DAVIS, S. H. 1979 *SIAM J. Appl. Maths* **37**, 1–19.